CIRP Annals - Manufacturing Technology 60 (2011) 133–136

Contents lists available at ScienceDirect

CIRP Annals - Manufacturing Technology

journal homepage: http://ees.elsevier.com/cirp/default.asp

Ultraprecision cutting of photoresist/gold composite microstructures

J. Yan

Department of Mechanical Systems and Design, Tohoku University, Sendai, Japan

Submitted by T. Nakagawa (1), Tokyo

ARTICLE INFO

Keywords:
Ultraprecision
Cutting
Microstructure

ABSTRACT

Ultraprecision cutting tests were performed on a photoresist/gold bump composite and cutting characteristics were investigated by examining the surface topography, chip formation, cutting force, and temperature. The cutting mechanisms depended significantly on the cutting speed, undeformed chip thickness, and tool geometry. At a high cutting speed, photoresist softening occurred, leading to chip adhesion on tool faces and burr formation on gold bumps. Two kinds of microfractures were identified in the photoresist cutting, and critical cutting conditions for each were obtained. The findings in this study provide process criteria for ultraprecise planarization of LSI substrates for three-dimensional chip implementing technology.

1. Introduction

Three-dimensional implementation of large-scale integrated (LSI) chips is a key technology in the current rapidly advancing information-based society [1–3]. LSI chips are usually stacked and pressure-bonded via micro gold bumps electroplated on silicon wafers. Due to the low strength of the LSI chips, pressure-bonding is performed under a low load to prevent damage to the chips. For this reason, the bonding surfaces of the bumps need to be precisely flattened. To avoid contamination, photoresist, which is used as a mask in the bump electroplating, needs to be flattened together with the bumps and removed after the planarization step. The conventional planarization method is chemo-mechanical polishing (CMP) [4], in which the material removal rate in the centre region of the bump tends to be higher than in the fringe area, leading to a concave bump surface. Low efficiency and chemical pollution are also problems to be solved in CMP. In this work, ultraprecision cutting (diamond turning) is proposed as an alternative planarization method. In cutting of the two distinctly different materials, a few possible problems could occur. One is that as gold is a highly ductile material, burrs might be generated around the bump, which leads to short-circuiting of LSI chips. Another is that the significant thermoplasticity of the photoresist might affect the cutting of the bumps. In this study, cutting tests were performed on a photoresist/gold bump composite under various conditions, and fundamental cutting characteristics were investigated. The feasibility of ultraprecise bump planarization by diamond turning was demonstrated.

2. Experimental procedures

Cutting tests were performed using an ultraprecision lathe Nachi ASP-15. Fig. 1 shows a schematic of the experimental system. To prepare workpieces, first, a photoresist layer (thickness ~30 μm) was spin-coated on silicon wafers (diameter 150 mm) to provide masks for bump electroplating. After exposure and development of the photoresist, gold bumps (size: 80 μm × 30 μm × 20 μm) were plated on the silicon wafers. The pitch between the bumps was 20 μm. In addition, silicon wafers coated with photoresist only were also used as workpieces to examine the cutting characteristics of the photoresist. The workpiece was vacuum-chucked to the air spindle of the lathe, and dry cutting was carried out to avoid contamination from the coolant. A three-component dynamometer, Kistler 9317A, was used to measure the cutting forces. A thermography system, Chino Thermoview CPA7000, was used to measure the cutting temperature. Single crystalline diamond tools with nose radii of 10 mm were used for the experiments. The cutting model is schematically shown in Fig. 2, and the cutting conditions used are listed in Table 1.

3. Results and discussion

3.1. Correlation in cutting characteristics of two materials

The preliminary experiments demonstrated that the cutting characteristics of gold bumps were strongly dependent on those of the photoresist. For example, Fig. 3 shows scanning electron microscope (SEM) micrographs of two workpiece surfaces. In Fig. 3(a), many microfractures are seen on the photoresist surface, and significant burr formation can be confirmed around the bumps. In contrast, in Fig. 3(b), the photoresist surface is less fractured and no obvious burr formation can be seen around the bumps. The dependence of bump burr formation on photoresist microfractures was repeatable over a wide range of experimental conditions. This indicates that the cutting characteristics of the two materials are closely correlated. Thus, to improve the planarization quality of the bumps, it is important to clarify the cutting characteristics of the photoresist.

3.2. Effect of cutting speed on photoresist cutting

Cutting tests were performed on photoresist-coated wafers at various cutting speeds. Fig. 4 shows Nomarski micrographs of the

0007-8506/$ – see front matter © 2011 CIRP.
doi:10.1016/j.cirp.2011.03.129

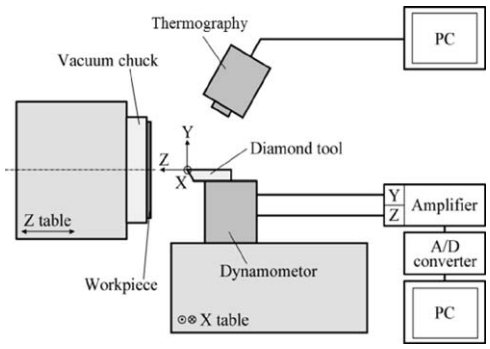

Fig. 1. Schematic diagram of the experimental system.

machined surface at different radial positions on the wafer. In the inner region, where the cutting speed is low, the surface is free from fractures, whereas in the outer region, where the cutting speed is high, numerous fractures are observed. In order to quantitatively evaluate the degree of fracture generation, an image processing computer program was used to calculate the percentage of the fractured surface area.

Fig. 5(a) shows the change in the percentage of the fractured area with cutting speed V_c. Microfractures begin to form to a significant degree when the cutting speed is higher than 300 m/min. Fig. 5(b) shows changes in the cutting temperature with cutting speed. As the cutting speed increases, the cutting temperature increases gradually from room temperature to over 40 °C. It should be pointed out that the temperature measured by thermography might be somewhat lower than the actual temperature in the cutting region due to the fact that the thermography measurement method is non-invasive and involves complicated error sources [5]. Fig. 5(c) shows changes in cutting forces as a function of cutting speed. As the cutting speed increases, both principal force and thrust force decrease.

High cutting speed might cause two effects in a photoresist, thermally induced softening/melting and high strain-rate induced embrittlement [6–8]. These two effects may coexist, and the predominance of either depends on the material composition and thermomechanical properties of the photoresist. Fig. 6 shows an SEM micrograph of the tool edge after a face turning cycle. Chip

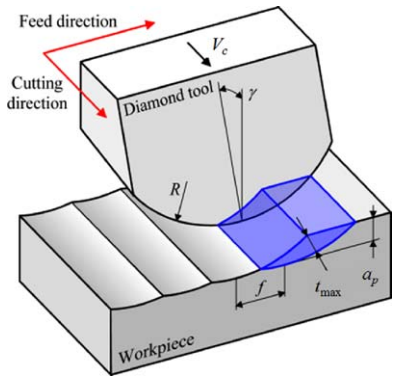

Fig. 2. Cutting model for a round-nosed diamond tool.

Table 1
Cutting conditions.

Workpiece	Photoresist/gold bump composite
Cutting tool	Single-crystal diamond tool
Nose radius R [mm]	10
Rake angle γ [°]	0, 15, 30
Relief angle α [°]	10
Edge radius r_e [nm]	50, 200
Depth of cut a_p [μm]	2, 4, 8, 16
Tool feed rate f [μm/rev]	10, 20, 40, 80
Spindle rotational rate n [rpm]	500, 1000, 1500, 2000, 2200

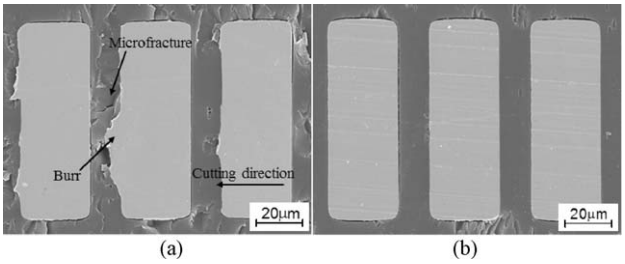

Fig. 3. SEM micrographs of two diamond-turned surfaces, showing correlation between bump burr formation and photoresist microfracture.

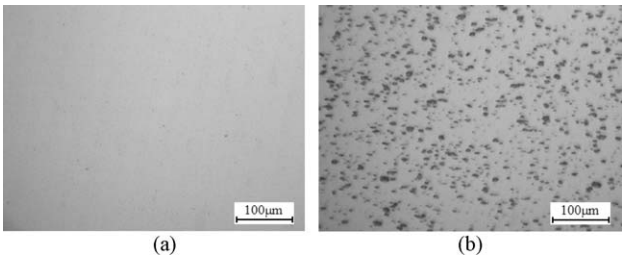

Fig. 4. Nomarski micrographs of a machined surface at different radial positions of the workpiece: (a) inner region, (b) outer region.

adhesion is seen on the tool rake face, indicating that photoresist melting occurred during cutting due to temperature rise [9]. Thus, thermally induced softening/melting might be predominant in this study, and material softening led to a decrease in cutting forces, as shown in Fig. 5(c). After cutting, however, the photoresist will undergo shrinking and hardening. Thus, tensile stress is induced leading to microfracture generation, as schematically shown in Fig. 7. Therefore, thermal microfracture generation is dominant at high cutting speeds. In this case, chip adhesion on the tool face will obstruct the chip flow when cutting gold bumps, causing burr formation at the bump edges.

To confirm the thermally induced softening phenomenon in the photoresist, thermomechanical property tests were performed using a Perkin Elmer tester, TMA-7, by indenting the photoresist with a quartz probe having a diameter of 3 mm at a load of 5 mN. The temperature was changed from room temperature to 100 °C at a rate of 5 °C/min. The tests were performed in a nitrogen atmosphere. As shown in Fig. 8, the photoresist begins to soften at a temperature of approximately

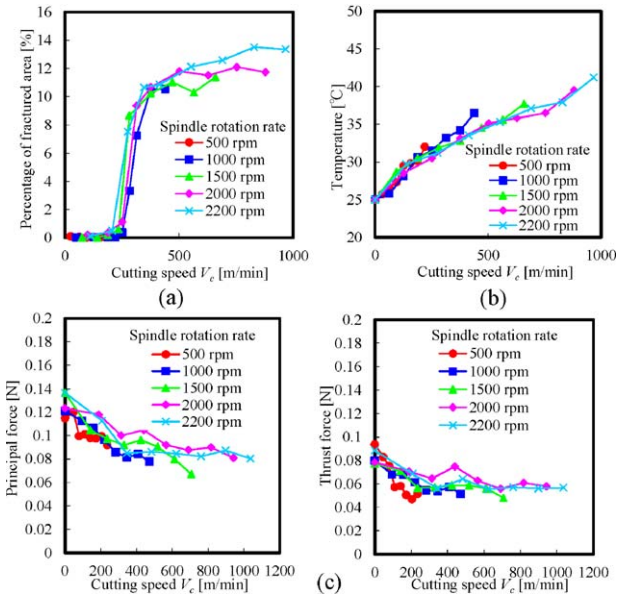

Fig. 5. Effects of cutting speed on (a) percentage of fractured area, (b) cutting temperature, and (c) cutting forces.

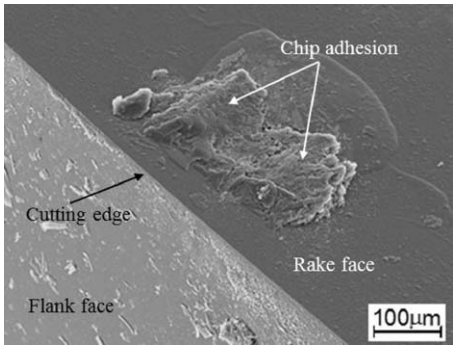

Fig. 6. SEM micrograph of tool edge showing chip adhesion.

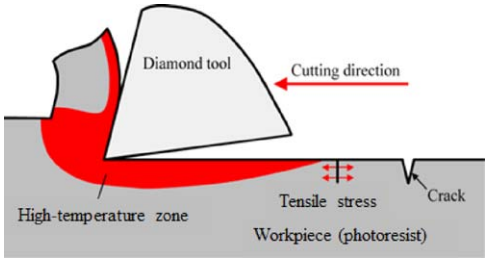

Fig. 7. Model for microfracture generation in photoresist cutting.

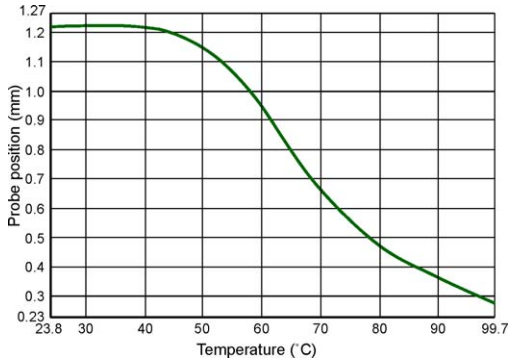

Fig. 8. Result of thermomechanical property test of the photoresist.

40 °C, and the higher the temperature, the softer is the photoresist. This result agrees well with the cutting force data in Fig. 5(c).

3.3. Effect of depth of cut and tool feed rate

Fig. 9 shows the change in percentage of the fractured area as a function of the depth of cut. As the depth of cut increases, microfracture generation of the photoresist becomes significant even at a low cutting speed. When the depth of cut was over 16 μm, fractures were observed on almost the entire wafer. Fig. 10 shows results for various tool feed rates. The general trend in Fig. 10 is similar to that in Fig. 9. In diamond turning with a round-nosed tool, both depth of cut a_p and tool feed rate f are directly related to the same parameter, the maximum undeformed chip thickness t_{max}, as shown in Fig. 2 and described by Eq. (1):

$$t_{max} = f\sqrt{\frac{2a_p}{R} + \frac{{a_p}^2}{R^2}} \quad (1)$$

Thus, the results in Figs. 9 and 10 indicate that microfracture generation becomes significant as the undeformed chip thickness increases. This cutting characteristic is very similar to that of a nominally brittle material.

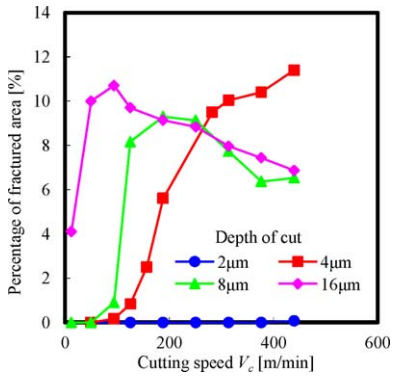

Fig. 9. Effect of depth of cut on photoresist microfracture.

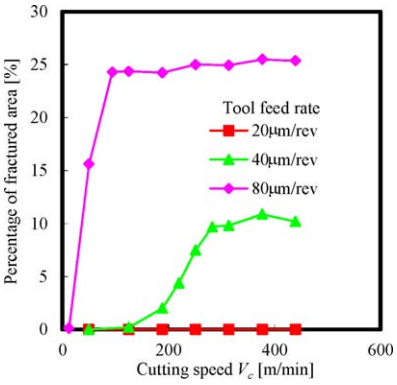

Fig. 10. Effect of tool feed on photoresist microfracture.

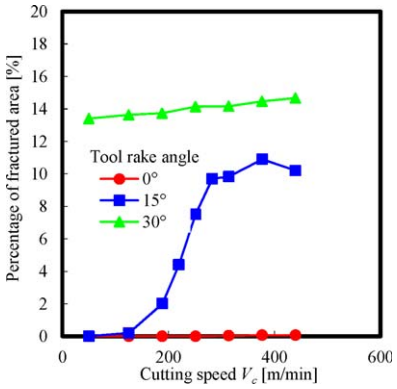

Fig. 11. Effects of tool rake angle on photoresist microfracture.

3.4. Effect of tool rake angle

Diamond tools having rake angles of 0°, 15°, and 30° were used in the experiments. Fig. 11 shows a plot of percentage of fractured area as a function of the tool rake angle. The percentage of fractured area increases dramatically with the tool rake angle. For the 30° rake angle, microfractures were generated over the entire workpiece surface. A high rake angle enhances tensile stress in the cutting region, which causes a brittle material to fracture; the results in Fig. 11 demonstrate again that the photoresist has a brittle nature. Therefore, microfractures generated at a high rake angle, a large depth of cut, and a high tool feed rate are due to non-thermal reasons, which are distinctly different from the microfracture generation at a high cutting speed.

3.5. Critical undeformed chip thickness

Fig. 12 shows SEM micrographs of cutting chips generated at depths of cut $a_p = 2$ μm and $a_p = 16$ μm (cutting speed

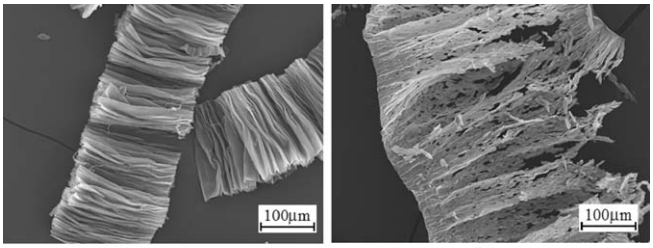

Fig. 12. SEM micrographs of cutting chips obtained at depth of cuts of (a) 2 μm and (b) 16 μm.

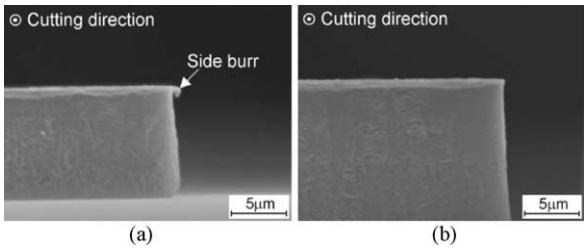

Fig. 13. SEM micrographs of side burr formation when cutting at different depths of cut of (a) 16 μm and (b) 2 μm.

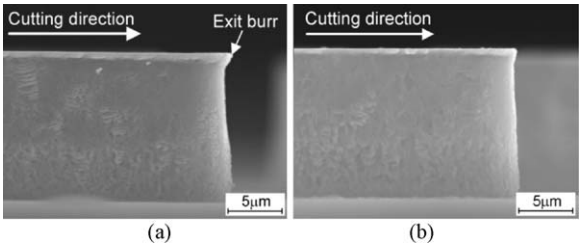

Fig. 14. SEM micrographs of exit burr formation when using diamond tools having different edge radii: (a) 200 nm and (b) 50 nm.

V_c = 200 m/min). At a_p = 2 μm, the chips are completely continuous. In contrast, at a_p = 16 μm the right side of the chip (larger undeformed chip thickness) is fragmented, while the left side (smaller undeformed chip thickness) remains continuous. Using the cutting model shown in Fig. 2 and SEM observations, the critical undeformed chip thickness for microfracture was estimated to be t_c = 0.7 μm.

3.6. Composite microstructure cutting

Next, the photoresist/gold bump composite microstructure was machined, and the effects of cutting parameters on bump burr formation were investigated. To observe burr formation, after cutting, the photoresist was removed with acetone. The side burr formation was found to be significantly affected by the depth of cut, while exit burr formation depended on the tool edge radius. For example, Fig. 13(a) and (b) shows SEM micrographs of bumps machined at a_p = 16 μm and a_p = 2 μm, respectively. A big side burr can be seen at the bump edge in Fig. 13(a), while no obvious burr can be seen in Fig. 13(b). Fig. 14 shows SEM micrographs of bumps machined by diamond tools having edge radii of 200 nm and 50 nm. The size of the exit burr became smaller with decreasing tool edge radius. Therefore, to prevent bump burr formation, it is important to use a sharp tool at a small depth of cut and a low tool feed rate, which is similar to the findings in the cutting of other metals [10,11]. Fig. 15 shows SEM micrographs of

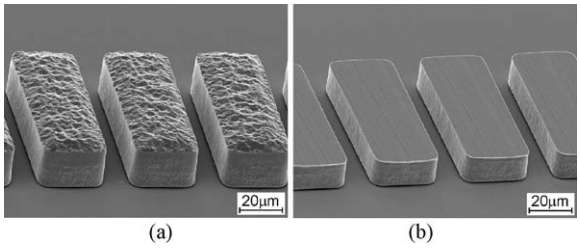

Fig. 15. SEM micrographs of gold bumps (a) before and (b) after diamond turning.

bumps before and after cutting. Before cutting, the bump surface was very rough, and after cutting, the surface becomes distinctly smoother. The surface roughness is 18 nm Ry and the flatness is 43 nm after cutting. The diamond-turned bumps can be directly used for low-pressure bonding in LSI implementation.

4. Conclusions

A photoresist/gold bump composite was diamond-turned to perform bump planarization. There is strong correlation between the cutting characteristics of the two materials. When the cutting speed is high, the photoresist is thermally softened and adheres to the tool rake face, which causes burr formation at bump edges and thermal fractures in the photoresist. The cutting mode of the photoresist transitions from ductile to brittle with increasing depth of cut, tool feed rate, and tool rake angle. The critical undeformed chip thickness for this ductile–brittle transition is 0.7 μm at a cutting speed of 200 m/min. In the cutting of the gold bump, the side burrs increase with depth of cut, and the exit burrs increase with tool edge radius. Under optimal conditions, ultraprecise bump planarization was realized.

Acknowledgement

The author would like to thank T. Sasaki (Kitami Institute of Technology) for assistance in experiments. Thanks are also extended to K. Tsurushima, Y. Kimura, A. Kawai, and K. Arai (DISCO Corporation) for providing experimental samples and technical cooperation.

References

[1] Brussel HV, Peirs J, Reynaerts D, Delchambre A, Reinhart G, Roth N, Weck M, Zussman E. (2000) Assembly of Microsystems. *Annals of the CIRP* 49(2): 451–472.
[2] Pavlidis VF, Friedman EG, 2009. Three-dimensional Integrated Circuit Design (Systems on Silicon), Elsevier.
[3] Feldmann K, Franke J, Schüßler F (2010) Development of Micro Assembly Processes for Further Miniaturization in Electronics Production. *Annals of the CIRP* 59(1):1–4.
[4] Zantye PB, Kumar A, Sikder AK (2004) Chemical Mechanical Planarization for Microelectronics Applications. *Materials Science and Engineering R Reports* 45(3–6):89–220.
[5] Davies MA, Ueda T, M'Saoubi R, Mullany B, Cooke AL (2007) On the Measurement of Temperature in Material Removal Processes. *Annals of the CIRP* 56(2):581–604.
[6] Kobayashi A (1967) *Machining of Plastics*. McGraw-Hill, New York.
[7] Carr JW, Fegera C (1993) Ultraprecision Machining of Polymers. *Precision Engineering* 15(4):221–237.
[8] Xiao KQ, Zhang LC (2002) The Role of Viscous Deformation in the Machining of Polymers. *International Journal of Mechanical Sciences* 44(11):2317–2336.
[9] M'Saoubi R, Chandrasekaran H (2005) Innovative Methods for the Investigation of Tool–Chip Adhesion and Layer Formation during Machining. *Annals of the CIRP* 54(1):59–62.
[10] Aurich JC, Dornfeld D, Arrazola PJ, Franke V, Leitz L, Min S (2009) Burrs Analysis, Control and Removal. *Annals of the CIRP* 58(2):519–542.
[11] Stoll A, Leopold J, Neugebauer R (2006). Hybrid methods for analyzing burr formation in 2D-orthogonal cutting. In: Proceedings of the 9th CIRP Workshop on Modeling of Machining Operations, pp. 441–448.